Study of terahertz interferometric imaging using optical techniques

Yuntao He (何云涛)*, Yuesong Jiang (江月松), Yuedong Zhang (张跃东), and Guoli Fan (樊国丽)

School of Electronic and Information Engineering, Beihang University, Beijing 100191, China

**E-mail: taoyunhe@ee.buaa.edu.cn*

Received October 30, 2009

Principles of terahertz (THz) interferometric synthetic aperture imaging with heterodyne and optical techniques are presented. A THz interferometric experiment based on optical up-conversion is set up. The received THz signal is modulated into an optical carrier and transmitted in a fiber. To simulate phase differences between two THz receivers, the output of receiver is divided and a phase shifter is placed before electro-optical modulation (EOM). Interferometric spectra of these modulated optical signals are examined at different phase shifts. Otherwise, carrier suppression and phase error calibration are discussed for THz interferometric synthetic aperture imaging.

OCIS codes: 110.3175, 040.2235, 280.6730.

doi: 10.3788/COL20100802.0162.

Defined by frequencies from 0.1 to 10 THz, terahertz (THz) radiation is opening the door to a wide variety of applications. Waves in this gap are able to penetrate materials such as plastics, cloth, packaging, paper, and many organic compounds, including human tissues, but strongly absorbed by metals and other inorganic substances[1]. This means that imaging in THz frequencies can potentially reveal the presence of concealed objects such as knives and guns and also smuggled items such as drugs, alcohol, and money. Without the hazards associated with ionizing radiation, THz radiation computed tomography (T-rays CT) has been developed to substitute for X-rays[2]. So THz imaging can be widely used in astronomy, military, non-destructive testing (NDT), healthcare, aerospace, and communication[1−6].

Compared with the long history of microwave and optical imaging, THz imaging system has just emerged very recently. The THz wave imaging system was demonstrated by using THz time-domain spectroscopy (TDS) by Hu *et al.*[7]. These initial images have inspired a great deal of excitement and much of the subsequent development of THz imaging systems and techniques[8−12]. The simplest and most prevalent THz imaging configuration is the single-point measurement using a single transmitter and detector pair. To exceed diffraction limitation and increase the resolution, synthetic aperture technology was widely adopted in microwave, and optical region was proposed in THz imaging system[9−11]. The THz synthetic aperture imaging system was set up for astronomy in Ref. [13]. A synthetic phased-array THz imaging system was demonstrated by O'Hara *et al.*[9,10]. Federici has been dedicated in real-time THz interferometric and synthetic aperture imaging for many years[11,14−16], and an imaging array acquired video-rate images with four THz receivers was reported recently[16]. The principle of this approach is based on the fact that the coherent product (correlation) of the signal from pairs of THz receivers measured at different antenna-pair spacings (baselines) yields a sample point in the Fourier transform of the field of view (FOV), and the FOV itself is reconstructed by inverting the sampled points. To implement this, THz frequencies are down-converted and $N^*(N\text{-}1)/2$ correlators are need for an N-element array[17−19].

An alternative approach of imaging is to convert the received signals up to the optical carrier, transmit them in fiber and image them by coherent optical beam forming[20−23]. There are many advantages such as easiness of realizing real-time imaging, light weight and small scale, and low cost[24]. For THz synthetic aperture interferometric imaging based on optical technique, a key problem is to preserve the phase differences of each two receiver pairs. So the phase errors must be calibrated and the useless part of carrier should be filtered before beam forming.

In this letter, principles of THz synthetic aperture imaging with or without optical techniques are discussed. An experiment is set up to demonstrate the primary interferometric process and phase differences maintaining. The relations between interfered results and the phase difference are analyzed. And two important issues, phase error calibration and carrier suppression, are discussed and demonstrated.

The process of THz interferometric synthetic aperture imaging is described as follows. Firstly, the scattered and radiated THz waves received from FOV are converted to an intermediate frequency (IF) and transport along coaxial cables. Secondly, containing the amplitudes and phases of incident THz wave, these IF signal pairs are cross-correlated and integrated to yield spatial frequency samples[14,17−19]. Finally, the image of FOV is reconstructed by a proper inverse algorithm and post treatment. Figure 1 shows a scheme of THz synthetic aperture imaging system with frequency down-conversion.

Imaging system of this scheme has been widely used in radio astronomy at all kinds of frequencies including THz wave band. For a non-redundant N-element interferometric imaging array, there are $N^*(N\text{-}1)/2$ independent baselines (spatial frequency samples). It means that to figure out all the cross-correlations, $N^*(N\text{-}1)/2$ correlators are needed, which is square multiple of the receiver number. Besides, it would result in increasing bulk and electromagnetic interference especially in a complex environment for signals are transmitted in

 © 2010 Chinese Optics Letters

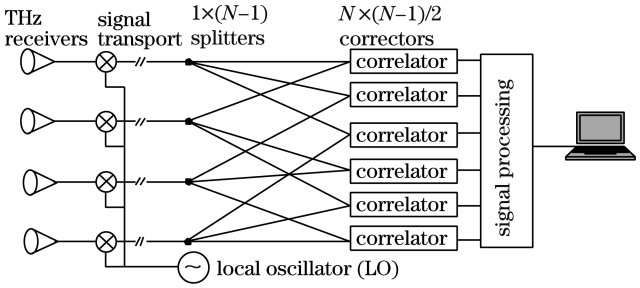

Fig. 1. The diagram of synthetic aperture imaging system using frequency down-conversion.

coaxial cables. These cross correlations (u-v samples) are processed with inverse algorithm and the image of FOV is obtained. Phase calibration is one of the most important procedures in the image reconstruction. Self-calibration and redundant spacings calibrations are comprehensively utilized[16,20,23].

In synthetic aperture imaging system, received signals should be modulated to a suitable frequency for transmitting and processing. One of the solutions is to down-convert the signal frequency so that the signal can be transmitted in coaxial-cable, which is applied in most cases at present[17−19]. Another method is frequency up-conversion which means modulating received signals to optical carriers and transmitting in fiber[20−24]. Transmission in optical fiber has many advantages such as wide bandwidth, low attenuation, and anti-interference to electromagnetism. Besides, scaled fiber arrays can be formed to image directly, no need to demodulate the optical signal. Compared with the heterodyne imaging method, up-conversion technique avoids large amount of correlators which increases with the number of receivers in geometric series. By using optical transmission and optical beam forming, the imaging system is much more efficient, simple, and economical.

The scheme of THz synthetic aperture imaging system using up-conversion is shown in Fig. 2. Received signals are amplified and transmitted into electro-optical modulators (EOM) where optical carriers are modulated. As optical carriers in all the fiber channels are provided by the same laser, these optical signals are coherent. At the end of fiber, optical signals are collimated and extended by a scaled lenslet array. The output of lenslet array is interfered with each other in space and focused on a charge-coupled-device (CCD) camera. So the image of FOV is obtained.

The radiation frequency (RF) input of EOM could be denoted as $E_{\rm r}(\theta,t)\cos(\omega_{\rm r}t+\varphi_{\rm r})$, where $E_{\rm r}(\theta,t)$ is the amplitude of the incident THz wave, θ is the incident angle, $\omega_{\rm r}$ is the output frequency from the receiver, and $\varphi_{\rm r}$ is the phase depended on the position of receiver. The modulated complex optical amplitude can be given as

$$E_{\rm o}=E_{\rm i}\exp\{{\rm j}(\omega_i+\varphi_i)+{\rm j}mE_{\rm r}(\theta,t)\cos(\omega_{\rm r}t+\varphi_{\rm r})\},\quad(1)$$

where $E_{\rm i}$ and $\omega_{\rm i}$ present the amplitude and frequency of the input carrier respectively, $\varphi_{\rm i}$ is the initial carrier phase, and m denotes the modulation constant determined by the properties of the EOM and the receiver. The phase shift of the output carrier $mE_{\rm r}(\theta,t)\cos(\omega_{\rm r}t+\varphi_{\rm r})$ is induced by the THz signal. Operating Jacobi-Anger expansion on the phase shift component, the amplitude of output optical is rewritten as[25]

$$E_{\rm o}=E_{\rm i}\exp\{{\rm j}(\omega_{\rm i}+\varphi_{\rm i})\}\cdot\exp\{{\rm j}mE_{\rm r}(\theta,t)\cos(\omega_{\rm r}t+\varphi_{\rm r})\}=E_{\rm i}\exp\{{\rm j}(\omega_{\rm i}+\varphi_{\rm i})\}$$
$$\times\sum_{n=-\infty}^{+\infty}{\rm j}^nJ_n[mE_{\rm r}(\theta,t)]\exp\{{\rm j}n(\omega_{\rm r}t+\varphi_{\rm r})\}=\sum_{n=-\infty}^{+\infty}{\rm j}^nE_{\rm i}J_n[mE_{\rm r}(\theta,t)]\exp\{{\rm j}(\omega_i+n\omega_{\rm r})t+{\rm j}(\varphi_{\rm i}+n\varphi_{\rm r})\}.\quad(2)$$

From Eq. (2), we can see that the modulation optical spectrums are distributed at $(\omega_{\rm i}+n\omega_{\rm r})$, and the amplitudes of these spectrum components are a function of the n-th order Bessel function of the first kind corresponded. When an optical band-pass filter centered at $(\omega_{\rm i}+\omega_{\rm r})$ is applied, the upper side band (USB) component is left behind. According to the approximation of Bessel function, the USB signal with a small modulation signal $(mE_{\rm r}(\theta,t))$, could be given as

$$E_{\rm USB}\approx\frac{1}{2}{\rm j}mE_{\rm i}E_{\rm r}\exp\{{\rm j}[(\omega_{\rm i}+\omega_{\rm r})t+(\varphi_{\rm i}+\varphi_{\rm r})]\}.\quad(3)$$

The USB signal transmitted in optical fiber is collimated by lenslet array at the end of fiber. So the optical field in the plane of collimated optical can be expressed as

$$\vec{U}(r,\theta)=U(r,\theta)\exp\{{\rm j}t(\omega_{\rm r}+\omega_{\rm i})+{\rm j}(\varphi_{\rm i}+\varphi_{\rm r})\},\quad(4)$$

where (r,θ) and $U(r,\theta)$ are the coordinate plane and the distribution of the collimated optical respectively. Then the optical in detector plane (x,y) is denoted as

$$\vec{U}_f(x,y)=\frac{\exp\{{\rm j}\kappa(x^2+y^2)/2f\}}{{\rm j}\lambda f}\times\iint_{(r,\theta)}\vec{U}(r,\theta)\times\exp\left\{-{\rm j}2\pi\frac{xr\cos\theta+yr\sin\theta}{\lambda f}\right\}r{\rm d}r{\rm d}\theta,\quad(5)$$

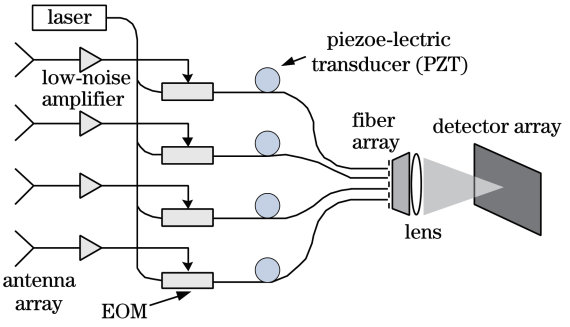

Fig. 2. The diagram of synthetic aperture imaging based on optical beam forming.

where κ denotes the wave number, λ is the wavelength, and f is the focus of imaging lens. For an n-element array, the interferometric optical field is expressed as

$$\boldsymbol{U}_{\text{interf}}(u,v) = \sum_{k=1}^{n} \boldsymbol{U}_f^{(k)}(x,y) \times \exp\{-\text{j}2\pi(xr_k\cos\theta_k + yr_k\sin\theta_k)\}. \quad (6)$$

The superscript and subscript k here denote sequence of receivers. Then the detected intensity is the square of absolute value of the interferometric optical field.

A primary experiment is set up to demonstrate the above theory. The scheme and actual system are shown in Figs. 3 and 4 respectively. The transmitter consists of a 500-GHz frequency quintupler and a 93-GHz varactor-tunable Gunn oscillator, while the LO of receiver is a 500-GHz backward wave oscillator (BWO). A superconductor-insulator-superconductor (SIS) mixer is applied in the THz receiver. The frequencies of the input and LO are 497.7 and 487.7 GHz respectively. The adjustable attenuator is used to set the RF input powers of the two 40 GHz phase EOMs (model: Covega Mach 40 066-40-P-A-A) identically, while the adjustable phase shifter is used to simulate the IF signal of the second receiver to produce phase differences. The spectrum line width of the distributed-feedback (DFB) laser is less than 10 kHz and the whole optical path is polarization-maintaining and single-mode. And an optical spectrum analyzer (OSA) is employed to measure the interferometric spectra.

The feedback loop, composing a PIN photo detector and a data acquisition card, is to correct the random relative phase errors in fiber. The output voltage of the PIN diode is dominated by the phase difference of optical carriers as there is almost no change in carrier power before and after the EOMs. The phase difference could be compensated by the feedback of changing relatively the optical phase in one of the EOMs. Since both the optical carrier and the sidebands experience the same optical length, then the phase error in sidebands could be compensated with the above feedback loop. The frequency of phase variants due to temperature, acoustics and stress-change in fiber is usually low, and tests show that a feedback loop of more than 15 kHz is enough to control the phase errors.

The experiment is to demonstrate phase difference preserving. From Eq. (3), we can get the expression of the interferometric optical intensity of two USB signals as follows:

$$I_{\text{USB}} = \frac{1}{2}m^2E_{\text{i}}^2E_{\text{r}}^2\left[1+\cos\left(\varphi_{\text{r1}}-\varphi_{\text{r2}}\right)\right]. \quad (7)$$

In the experiment, an IF of 10.03 GHz is captured with a –10.47-dBm output power by the THz receiver. It is inputted to the power coupling module (PCM) and divided equally. To simulate a parallel wave incidence to the THz receiver, the adjustable attenuator is turned to balance the powers into EOM. Then the bias voltage is changed to set phase differences of the EOM RF inputs, and the interferometric spectrums are observed and recorded.

Figure 5 shows the original optical spectrums at variant phase differences of EOM RF inputs from 0° to 180°, while Fig. 6 is the peak power chart of the optical upper side band that corresponds to the right-hand points at a 10.03-GHz deviation from the center wavelength of 1536.504 nm. The powers at the center wavelength of 1536.504 nm are also shown in Fig. 6.

The variation of the carrier power at 1536.504 nm (marked with triangle) in Fig. 6 is the interferometric intensity of the optical carrier. It shows the phase difference of the two modulated optical signals. The

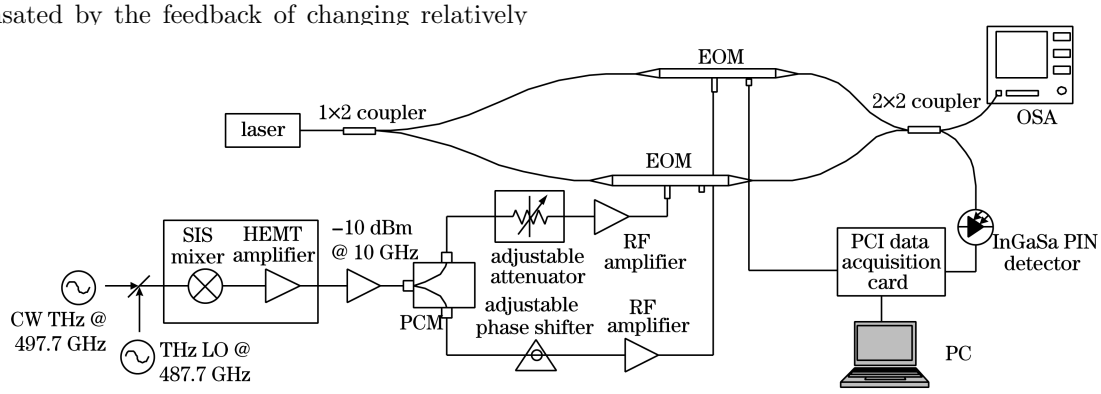

Fig. 3. Schematic representation of the experimental configuration.

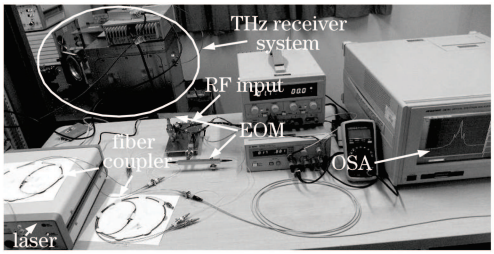

Fig. 4. Photo of actual experimental setup in the laboratory.

root mean square (RMS) of the fluctuation in the carrier power is about 0.1 dB, and this unevenness will create a phase error of 12.3° at most. So the phase error in optical domain is corrected well by utilizing the feedback loop with a frequency of 15 KHz. Then, the measured interferometric intensity of USB and LSB (marked with circle and square corresponding) illustrate the phase difference of EOM RF input without the influence of phase errors in optical domain. They coincide with the theory results. According to Eq. (7), the interferometric intensity of the

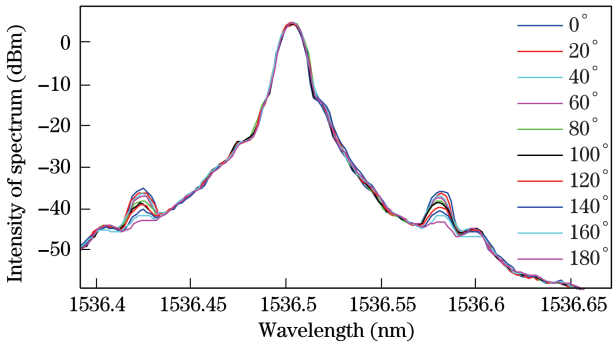

Fig. 5. Interferometric spectra of the EOM output modulated by THz receiver.

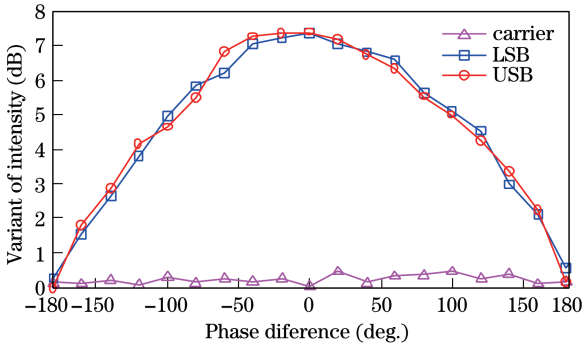

Fig. 6. The variant of peak powers of the optical upper side band and optical carrier.

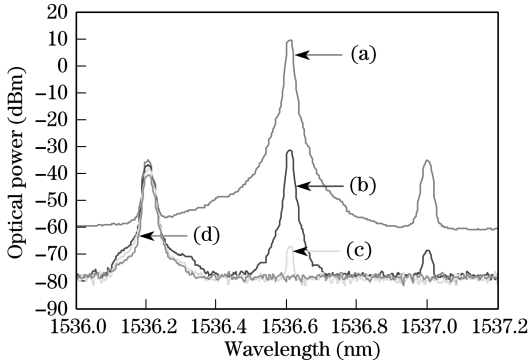

Fig. 7. Optical spectrum using FBG filters.

first two side bands is a cosine curve versus. the phase differences of EOM RF inputs from –180° to 180°. This means that the phase differences are preserved well during the transmission, which is one of the most important conditions in THz interferometric synthetic aperture imaging.

When one is working at visible, infrared, microwave, or THz frequency, to synthesize a good-quality image with an interferometric array, attentions must be paid to control the signal phase in path for each receiver channel to an accuracy of less than one tenth of a wavelength in order to achieve high quality images[26–28]. Any deviation in phase measurements at individual elements of the array, would lead to a severe degradation in the point-spread function of the system, and poor image quality. For the optical signals in fiber, phase errors induced by acoustic and thermal fluctuations change drastically, but show homology on carrier as well as both sidebands. This property can be used to calibrate the phase errors in optical domain by interfering the optical carriers with the same reference carrier[28].

As to phase errors induced by the receiver positions and other factors before receiving THz signals, phase calibration methods like redundant spacings calibration (RSC) and self-calibration algorithms must be adopted[26,27]. And for THz interferometric synthetic aperture imaging with optical technique advanced, self-calibration algorithm derived from closure imaging in radio astronomy may be more suitable as methods like RSC need phase shifts in optical transmission which would influence the phase calibration in optical domain as mentioned above.

Another important problem in the proposed imaging approach is to depress the carrier filter through the first side band[23]. If the intensity of carrier frequency part is comparative or even bigger than that of sidebands during interference, the interferometric image of these optical sideband frequencies will be covered by that of optical carrier frequencies in the infrared CCD. In order to suppress the carrier frequencies, one way is to utilize the optical carrier interferences in Mach-Zehnder (MZ) EOM. Other instruments including optical add-drop multiplexer (OADM) and thin-film filter are also used comprehensively. In our experiment, fibber Bragg grating (FBG) filter is utilized to depress optical carrier intensities.

Figure 7 shows spectra modulated by a 50-GHz oscillation with different FBG filters. The line (a) is the spectrum without any carrier suppression process. While lines (b), (c), and (d) are the corresponding spectra with one, two, and three FBG filters, respectively. In our experiment, the reflective insertion loss measured for each FBG filter is about 1.7 dB, while the reflective adjacent channel isolation reaches as large as 35 dB. So we can choose a proper stage number of the FBG filter to make sure the optical carrier does not degrade the imaging quality.

Inconclusion, THz imaging technology has a comprehensive application, and THz synthetic aperture imaging with optical technique improves the imaging speed and spatial resolution. Among the two interferometric manners in this letter, THz synthetic aperture imaging with optical up-conversion has many merits and the imaging process is analyzed deeply. From the interferometric spectra of optical signals modulated by THz signals, the phase differences are preserved well, and images of FOV could be formed with more receivers according to synthetic aperture principles. Based on interferometric imaging techniques, the phase errors induced before modulation can be corrected by self-calibration algorithm and RSC, while phase errors in optical domain have to be compensated by interfering of carrier and reference optical. Besides, problems of carrier suppression could be settled by MZ EOM and optical filters, and the experiments with FBG filters show pretty performances. The work in this letter indicates that real-time and high resolution THz imaging could be implemented by interferometric synthetic aperture system and optical up-conversion.

This work was supported by the National High-Tech Research and Development Program (No. 2007AA12Z114) and the Innovation Foundation of

BUAA for PhD Graduates. We are grateful to Shencai Shi and Zhenghui Lin in Purple Mountain Observatory of Chinese Academy of Sciences for their help in the THz receiver test.

References

1. P. H. Siegel, IEEE Trans. on Microwave Theory and Techniques **50,** 910 (2002).
2. J. Pearce, H. Choi, D. M. Mittleman, J. White, and D. Zimdars, Opt. Lett. **30,** 1653 (2005).
3. D. M. Mittleman, M. Gupta, R. Neelamani, R. Baraniuk, J. V. Rudd, and M. Koch, Appl. Phys. B **68,** 1085 (1999).
4. E. R. Brown, Int. J. High-Speed Electron. Systems **13,** 93 (2003).
5. W. L. Chan, J. Deibel, and D. M. Mittleman, Rep. Prog. Phys. **70,** 1325 (2007).
6. R. Bogue, Sensor Review **29,** 6 (2009).
7. B. B. Hu and M. C. Nuss, Opt. Lett. **20,** 1716 (1995).
8. Q. Wu and X.-C. Zhang, Appl. Phys. Lett. **67,** 3523 (1995).
9. K. McClatchey, M. T. Reiten, and R. A. Cheville, Appl. Phys. Lett. **79,** 4485 (2001).
10. J. O'Hara and D. Grischkowsky, Opt. Lett. **27,** 1070 (2002).
11. J. F. Federici, D. Gary, B. Schulkin, F. Huang, H. Altan, R. Barat, and D. Zimdars, Appl. Phys. Lett. **83,** 2477 (2003).
12. A. M. Sinyukov, Z. Liu, Y. L. Hor, K. Su, R. B. Barat, D. E. Gary, Z. Michalopoulou, I. Zorych, J. F. Federici, and D. Zimdars, Opt. Lett. **33,** 1593 (2008).
13. A. I. Sargent, W. J. Welch, Annu. Rev. Astro. Astrophys **31,** 297 (1993).
14. A. Bandyopadhyay, A. Stepanov, B. Schulkin, M. D. Federici, A. Sengupta, D. Gary, J. F Federici, R. Barat, Z. H. Michalopoulou, and D. Zimdars, J. Opt. Soc. Am. A **23,** 1168 (2006).
15. A. M. Sinyukov, A. Bandyopadhyay, A. Sengupta, R. B. Barat, D. Gary, Z. H. Michalopoulou, D. Zimdars, and J. F. Federici, Int. J. High-Speed Electron. Systems **17,** 431 (2007).
16. Z. Liu, K. Su, D. E. Gary, J. F. Federici, R. B. Barat, and Z. Michalopoulou, Appl. Opt. **48,** 3788 (2009).
17. C. S. Ruf, C. T. Swift, A. B. Tanner, and D. M. Le Vine, IEEE Trans. Geoscience and Remote Sensing **26,** 597 (1988).
18. M. Peichl, H. Suess, and M. Suess, Radio Science **33,** 781 (1998).
19. A. R. Thompson, J. M. Moran, and G. W. Swenson, *Interferometry and Synthesis in Radio Astronomy (*Wiley, New York, 2001).
20. P. M. Blanchard, A. H. Greenaway, A. R. Harvey, and K. Webster, J. Lightwave Technol. **17,** 418 (1999).
21. J. E. Leight and L. J. Lembo, Proc. SPIE **4112,** 126 (2000).
22. F. Schlottau, M. Colice, K. H. Wagner, and W. R. Babbitt, Opt. Lett. **30,** 3003 (2005).
23. C. A. Schuetz, J. Murakowski, G. J. Schneider, and D. W. Prather, IEEE Trans. Microwave Theory and Techniques **53,** 1732 (2005).
24. J. Capmany and D. Novak, Nature Photonics **1,** 319 (2007).
25. Y. He, Y. Jiang, and C. Wang, Acta Opt. Sin. (in Chinese) **28,** 1201 (2008).
26. T. J. Cornwell, Science **245,** 263 (1989).
27. A. Lannes and E. Anterrieu, J. Opt. Soc. Am. A **16,** 2866 (1999).
28. Y. He, Y. Jiang, and Y. He, Acta Opt. Sin. (in Chinese) **28,** (Suppl. 2) 38 (2008).